Available online at www.sciencedirect.com
ScienceDirect
International Journal of Multiphase Flow 34 (2008) 723–733
International Journal of Multiphase Flow
www.elsevier.com/locate/ijmulflow

Direct numerical simulation of particle dispersion in a turbulent jet considering inter-particle collisions

Jie Yan [a], Kun Luo [a,*], Jianren Fan [a,*], Yutaka Tsuji [b], Kefa Cen [a]

[a] State Key Laboratory of Clean Energy Utilization, Zhejiang University, Hangzhou 310027, China
[b] Department of Mechanophysics Engineering, Graduate School of Engineering, Osaka University Suita, Osaka 565-0871, Japan

Received 7 September 2007; received in revised form 6 December 2007

Abstract

To investigate the behaviour of inter-particle collision and its effects on particle dispersion, direct numerical simulation of a three-dimensional two-phase turbulent jet was conducted. The finite volume method and the fractional-step projection algorithm were used to solve the governing equations of the gas phase fluid and the Lagrangian method was applied to trace the particles. The deterministic hard-sphere model was used to describe the inter-particle collision. In order to allow an analysis of inter-particle collisions independent of the effect of particles on the flow, two-way coupling was neglected. The inter-particle collision occurs frequently in the local regions with higher particle concentration of the flow field. Under the influence of the local accumulation and the turbulent transport effects, the variation of the average inter-particle collision number with the Stokes number takes on a complex non-linear relationship. The particle distribution is more uniform as a result of inter-particle collisions, and the lateral and the spanwise dispersion of the particles considering inter-particle collision also increase. Furthermore, for the case of particles with the Rosin–Rammler distribution (the medial particle size is set $d_{50} = 36.7$ μm), the collision number is significantly larger than that of the particles at the Stokes number of 10, and their effects on calculated results are also more significant.

Keywords: Inter-particle collision; Hard-sphere model; Gas–solid two-phase turbulent jet; Direct numerical simulation; Particle dispersion

1. Introduction

Due to its particular flow characteristics, turbulent plane jet has attracted extensive attention for a long time. The fundamental study on it is helpful to the overall understanding of the turbulent flow dynamics. The particle-laden turbulent jet is also of practical interest because of its presence in a broad range of engineering applications such as combustion, aerosol reaction, jet propulsion and air pollution control. In these processes, the inter-particle collision, which is one of the most interesting problems in two-phase flows, plays an important role for improving the design of engineering systems and control the particle transport.

There have been many experimental and numerical studies of gas–solid two-phase turbulent jet flows over the past decades. Melville and Bray (1979) investigated the gas–solid two-phase jet flows and presented a simple model to characterize them. To predict the particle dispersion in particle-laden flows, Crowe et al. (1985, 1988) first proposed the use of the particle Stokes number which is the ratio of the particle aerodynamics response time to the time scale associated with the large-scale organized vortex structures in the free shear flows. They found that the particles with the smaller and the larger Stokes numbers have the uniform concentration distribution in the flow field, but the particles with the intermediate Stokes number of the order of unity concentrate in the outer boundary regions of the large-scale vortex structures with highest diffusivity. Thereafter, there are many related studies that obtain the similar conclusions (Longmire, 1994; Wicker and Eaton, 2001;

* Corresponding authors.
E-mail addresses: zjulk@zju.edu.cn (K. Luo), fanjr@zju.edu.cn (J.R. Fan).

0301-9322/$ - see front matter © 2008 Elsevier Ltd. All rights reserved.
doi:10.1016/j.ijmultiphaseflow.2008.02.004

Uchiyama and Naruseb, 2003; Luo et al., 2006). Hardalupas et al. (1989) investigated the velocity and particle flux characteristics of a turbulent particle-laden jet and found the mass mixture ratio has a little effect on the particle concentration distribution. The dispersion of non-evaporating droplet in a round jet was studied experimentally by Longmire and Eaton (1992). They found that particles of Stokes number which is between 1 and 10 concentrate largely in the high-strain-rate and low-vorticity regions. This non-uniform particle distribution is known as"preferential concentration" which was also observed by Eaton and Fessler (1994). Yuu et al. (1996) performed direct simulation of a gas-particle turbulent free jet with a low Reynolds number. They obtained relatively good agreement with their LDA experimental data.

All the above-mentioned simulations are based on the assumptions of dilute flow and the inter-particle collisions are neglected. But some studies showed that the inter-particle collisions may play an important role in the dilute two-phase turbulent flows. Tanaka and Tsuji (1991) simulated the gas–solid two-phase flow in a vertical pipe with accounting for inter-particle collision. They described inter-particle collision using the hard-sphere model with inter-particle collision calculated by a deterministic method and found that the inter-particle collision has large effect on the diffusion of particles even in dilute conditions in which particle volume fraction is $O(10^{-4})$. Sommerfeld and Zivkovic (1992) considered the inter-particle collision in dilute phase pneumatic conveying through pipe systems by applying a stochastic collision model. They revealed that inter-particle collision plays a non-negligible role even at low overall mass loading for the development of the particle concentration profiles. Oesterlé and Petitjean (1993) and Sommerfeld (1995) performed respectively the simulation of gas–solid flow in a horizontal pipe and channel and demonstrated the importance of inter-particle collisions. Thereafter, many researchers presented the similar conclusions (e.g., Lun and Liu, 1997; Sakiz and Simonin, 2001; Sommerfeld, 2003). Besides, there is some work on collision frequency in homogeneous isotropic turbulence. Sundaram and Collins (1997) performed one-way coupled DNS of isotropic particle-laden turbulent suspension to study the collision frequency. They found the collision frequency involves a complex interplay of the particle concentration and mechanisms responsible for relative motion between the particles. Wang et al. (1998a,b) performed numerical experiments to study the geometric collision rate of finite-size particles in isotropic turbulence and compared their results with theoretical predictions by Saffman and Turner (1956) and by Abrahamson (1975). It was found that although in very different manners, both the large-scale and small-scale fluid motion can contribute to the collision rate. Sommerfeld (2001) applied the stochastic collision model for inter-particle collisions in homogeneous isotropic turbulence and obtained consistent results.

Although there are some studies on the inter-particle collision in the homogeneous isotropic turbulence and the flows in pipes and channels, there is not the study of inter-particle collision in the spatially-developing turbulent jet to the authors' knowledge. In this study, we combine the DNS method and the hard-sphere model to study the inter-particle collisions for particles at different Stokes numbers in a three-dimensional spatially evolving plane jet. The main objective is twofold. Firstly, to reveal the characteristics of inter-particle collision for particles at different Stokes numbers. Secondly, to investigate the effects of the inter-particle collision on the particle dispersion and provide references for the application in related industries.

2. Mathematical descriptions

2.1. Flow configuration and boundary conditions

Fig. 1 shows the flow configuration of a three-dimensional gas–solid two-phase turbulent plane jet. The fluid is injected into the domain through the whole slot nozzle, but the particles are just injected through a square region located in the center of the slot with side length d. The fluid Reynolds number based on inflow velocity U_0 and nozzle width d is 3000. To include the largest vortex structures in the simulations, the length of the calculation region in the streamwise(x) and spanwise(z) directions $20d$ and $6.4d$ in the lateral direction(y). Initially, a shear layer with the velocity profile in the region with the nozzle width d at the inlet boundary is calculated according to the following typical top-hat shape velocity profile (Klein et al., 2003a,b):

$$\begin{aligned} u &= \frac{U_0}{2} + \frac{U_0}{2}\tanh\left(\frac{y}{2\theta_0}\right) \\ v &= 0 \\ w &= 0 \end{aligned} \tag{1}$$

in which U_0 is the initial streamwise inflow velocity, θ_0 is the initial momentum thickness selected as $0.05d$. u, v and w are, respectively, the streamwise, lateral and spanwise velocities. Outside the region of the nozzle width d, all the fluid velocities are set as zero. At the streamwise outflow boundary, Neumann boundary conditions for velocity and pressure are used and the pressure is also corrected. At the lateral boundaries, the pressure is set as zero. In the spanwise direction, the periodic boundary conditions are applied.

2.2. Fluid motion

To calculate the fluid flow, direct numerical simulation (DNS) was performed. The gas phase is regarded as an ideal, Newtonian fluid. And, two-way coupling effects are not considered in this study, which is a valid approach to analyse solely the inter-particle collision behaviour and to evaluate the effects of inter-particle collisions. The same model was used by Tanaka and Tsuji (1991) and Sommerfeld (2003). We will take into account two-way coupling between the fluid and particle phase in the future work.

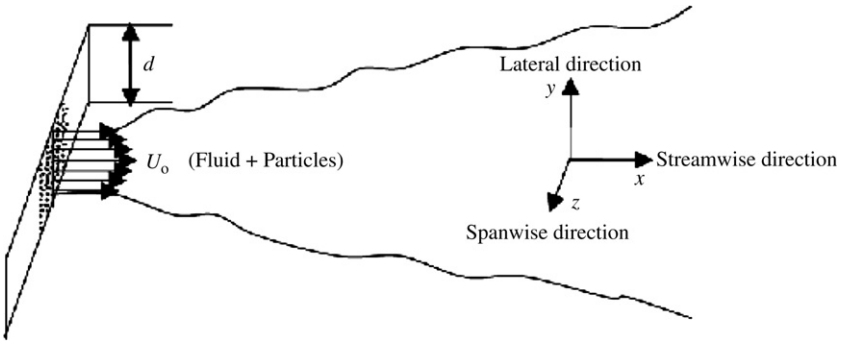

Fig. 1. Flow configure of the three-dimensional gas–solid two-phase turbulent jet.

When the body force is not included, the flow field can be calculated according to the following non-dimensional governing equations:

$$\text{Continuum equation}: \frac{\partial u_i}{\partial x_i} = 0 \tag{2}$$

$$\text{Momentum equation}: \frac{\partial u_i}{\partial t} + \frac{\partial u_i u_j}{\partial x_j} = -\frac{1}{\rho}\frac{\partial p}{\partial x_i} + \frac{1}{Re}\frac{\partial}{\partial x_j}\left(\frac{\partial u_i}{\partial x_j} + \frac{\partial u_j}{\partial x_i}\right) \tag{3}$$

in which, u_i, u_j and p are non-dimensional velocity and pressure; ρ is the density of the fluid; Re is the fluid Reynolds number given by $Re = U_0^* d/v$, where U_0 is inflow velocity, d is nozzle width and v is kinematic viscosity of fluid. And U_0 and d are the characteristic velocity and length scales, respectively. The reference density is the density of the air under the normal temperature and pressure.

The general requirements to simulate the turbulence using DNS are that the numerical techniques can provide the high accuracy in both space and time and can also solve the full N–S equations efficiently. The above governing equations are solved by the finite volume method and the fractional-step projection technique (Chorin, 1968). In the streamwise and spanwise directions, the uniform staggered grids are used; in the lateral direction, the uniform staggered grids are set in the region of $-2.25d < y < 2.25d$, outside this area the grids are stretched. The total grid points $200 \times 64 \times 128$ are used along x, y and z directions. Central differences are used for the spatial discretization to ensure the second-order precision of the solutions in space and a low-storage, third-order Runge–Kutta scheme is applied for time integration. The Poisson equation for pressure is solved using a direct fast elliptic method. For detailed numerical strategies, please refer to references (Klein et al., 2003a,b).

2.3. Particle motion

In the present work, the calculation of particle motion is divided into two progresses by using the uncoupling technique developed by Bird (1976). Firstly, the inter-particle collision is not to be considered at first and the motions of all particles are calculated by the governing equations mentioned later. Secondly, the occurrence of inter-particle collisions during the first step is examined for all particles. If a particle is found to collide with another particle, the motion of the collision pair is re-calculated using the post-collision velocities and their position is assumed to be changeless.

2.3.1. Particle motion without collision

To focus on the inter-particle collision and its effect on the particle dispersion, the influence of particles on fluid is neglected. All individual real particles are tracked in the Lagrangian framework based on one-way coupling. Due to the material density of particles is far larger than the density of the fluid, the minor force terms such as the virtual mass, the buoyancy, the Basset and the Magnus forces can be neglected (Stock, 1996; Vojir and Michaelides, 1994). Considering only the Stokes drag, the non-dimensional governing equations for determining the particle momentum and position are, respectively,

$$\frac{\mathrm{d}\boldsymbol{u}_\mathrm{p}}{\mathrm{d}t} = \frac{f}{St}(\boldsymbol{u}_\mathrm{f} - \boldsymbol{u}_\mathrm{p}) \tag{4}$$

$$\frac{\mathrm{d}\boldsymbol{x}}{\mathrm{d}t} = \boldsymbol{u}_\mathrm{p} \tag{5}$$

where $\boldsymbol{u}_\mathrm{p}$ is the particle velocity vector and $\boldsymbol{u}_\mathrm{f}$ is the fluid velocity vector at the position of the particle. $f$is the modified factor for the Stokes drag force, which can be described by $f = 1 + 0.15Re_\mathrm{p}^{0.687}$ when $Re_\mathrm{p} \leqslant 1000$ (Clift et al., 1978). The particle Reynolds number $Re_\mathrm{p} = |\boldsymbol{u}_\mathrm{f} - \boldsymbol{u}_\mathrm{p}|d_\mathrm{p}/v$ (d_p is particle diameter, v is kinematic viscosity of fluid). The particle Stokes number St is defined as $St = \frac{\rho_\mathrm{p} d_\mathrm{p}^2/(18\mu)}{d/U_0}$ (ρ_p is the density of the particle, μ is the fluid dynamics viscosity). The velocity and position of the particle can be obtained by integrating Eqs. (4) and (5). The fluid velocity at the position of particle is obtained by using the third-order Lagrangian interpolating polynomials.

2.3.2. Inter-particle collision

In the simulation, the numerical algorithm of inter-particle collision is a key issue, because it greatly affects the whole computation time. Considering the particle number density is so low in the present work that a statistical

method to represent the inter-particle collision (Yonemura et al., 1993) is not appropriate, so we use the deterministic hard-sphere model (Tanaka and Tsuji, 1991). This model is based on the following ideas: (a) particles are rigid spheres (i.e. any persistent particle deformation during a collision is absent); (b) particles can interact each other only through binary collisions because particle concentration is sufficiently low that binary collisions are overwhelming; (c) inter-particle collisions are considered as instantaneous inelastic ones.

It should be noted that the foundation stone of the hard-sphere model is the law of conservation of momentum. This approach for treatment of inter-particle collision is based on kinematics, in which what would arise during collision processes is not considered in detail. Instead, this model focuses on what have changed after the collisions. Thus, the solution for the collision is carried out based on just a figure of geometrical relative displacements and any other kinetic relative parameters, like apparent mass, are not considered. Moreover, energy loss during the collision process is taken into account by the coefficient of restitution e which is included by this model. The model applied for the present study is appropriate, because the particle concentration is very low and the collision process is instantaneous, the particles are viewed as rigid ones and the occurrence of many-body collision is scarce, which is validated by Tanaka and Tsuji (1991) and Yamamoto et al. (2001). The main procedures are as follows.

2.3.2.1. Grid index method. There are N_p particles in the computational domain, and each individual particle may collide with any other particle theoretically. Then identification of particle collisions requires examining $N_p(N_p-1)/2$ particle pairs, therefore, it is terribly inefficient to go through the entire list of particles in order to identify colliding particles of a given particle. Moreover, the time step Δt in the present numerical algorithm is so small that each particle can only collide with neighboring particles during one time step. Consequently, we can examine a reduced subset of possible colliding particles and improve the computing efficiency by using optimum grid-index method. The specific method is as follows: in the computational domain a uniform grid spacing with the side-length of the grids in three directions $l_i (i = 1, 2, 3) \geqslant u^i{}_{p\,max}\Delta t$ is used, where $u^i{}_{p\,max}$ is the maximum component in three directions of the particle velocity. This suggests the potential collision particles for a given particle in any grid are found in the neighborhood comprising that grid and the 26 grids that surround the central grid ABCD–EFGH, as shown in Fig. 2. More details can be found in the literature (Sundaram and Collins, 1996).

2.3.2.2. Collision detection. Now let us identify whether inter-particle collision occurs during one time step Δt. Each particle is assumed to move with a constant velocity during this time step. Fig. 3 shows the relative motion particle j to i when they collide, where $\boldsymbol{r}_{R0}$ is the relative position vector

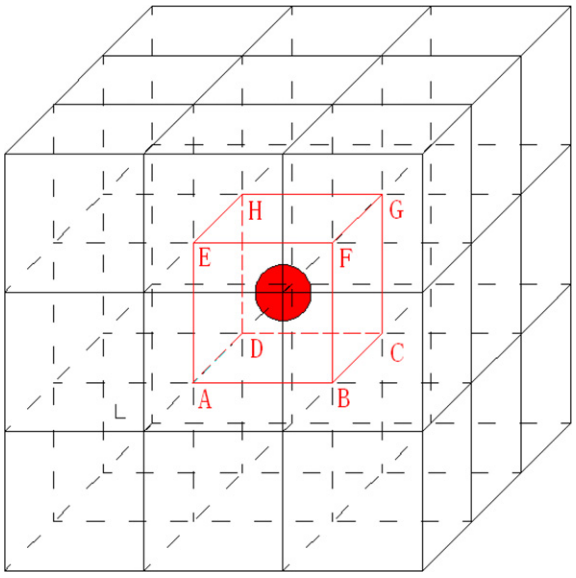

Fig. 2. Sketch of the 27 neighborhood cells.

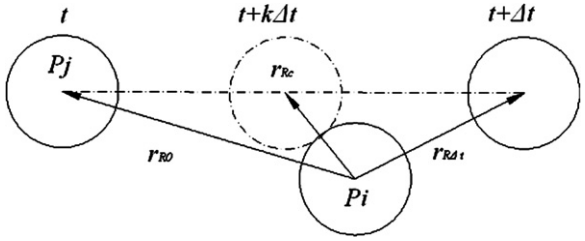

Fig. 3. Sketch of the relative motion between two particles.

at time t and $\boldsymbol{r}_{R\Delta t}$ is the relative position vector after Δt. The relative position vector of the collision point between the two particles is given by $\boldsymbol{r}_{Rc} = \boldsymbol{r}_{R0} + k(\boldsymbol{r}_{R\Delta t} - \boldsymbol{r}_{R0})$, where k represents a time scale factor. Inter-particle collision has occurred during this time step when the following equation for k has two real roots k_1 and $k_2 (k_1 < k_2, 0 \leqslant k_1 < 1)$:

$$|\boldsymbol{r}_{R0} + k(\boldsymbol{r}_{R\Delta t} - \boldsymbol{r}_{R0})|^2 = d_p^2 \tag{6}$$

where $|\boldsymbol{r}_{R0} + k(\boldsymbol{r}_{R\Delta t} - \boldsymbol{r}_{R0})|$ is the relative distance between the two particles. The potential inter-particle collisions mentioned above are located by evaluating the roots of Eq. (6).

When inter-particle collision occurs, the post-collision velocities $\boldsymbol{u}'_p$ of the two particles i and j can be obtained according to the equations of impulsive motion:

$$\boldsymbol{u}'_{pi} = \boldsymbol{u}_{pi} + \boldsymbol{J}/m_p \tag{7}$$

$$\boldsymbol{u}'_{pj} = \boldsymbol{u}_{pj} - \boldsymbol{J}/m_p \tag{8}$$

In the above equations, $\boldsymbol{u}_{pi}$ and $\boldsymbol{u}_{pj}$ are the pre-collision velocities of the two particles i and j, m_p is the particle mass, $\boldsymbol{J}$ is the impulsive force exerted on particle i. Based on the above assumptions, $\boldsymbol{J}$ can be expressed from (Tanaka and Tsuji, 1991):

$$\boldsymbol{J} = J_n\boldsymbol{n} + J_t\boldsymbol{t} \tag{9}$$

$$J_n = (1+e)M\boldsymbol{c}\bullet\boldsymbol{n} \tag{10}$$

$$J_t = \min\left[-\mu_f J_n, \frac{2}{7}M|\boldsymbol{c}_{fc}|\right] \tag{11}$$

$J_n\boldsymbol{n}$ and $J_t\boldsymbol{t}$ are the normal and the tangential components of the impulsive force $\boldsymbol{J}$. $\boldsymbol{n}$ is the normal unit vector of the relative position vector of the collision point between the two particles, $\boldsymbol{t}$ is the tangential unit vector in the direction of the relative velocity of the particle j to i, e is the coefficient of restitution ($e = 0.9$ in present work), $M = m_p/2$ for inter-particle collision and μ_f is the coefficient of friction. The pre-collision relative velocity of the particle j to i is given $\boldsymbol{c} = \boldsymbol{u}_{pj} - \boldsymbol{u}_{pi}\cdot\boldsymbol{c}_{fc}$ is the tangential component of the pre-collision relative velocity $\boldsymbol{c}$.

The motion of particles of the collision pair in the time step $\Delta\boldsymbol{t}$ is re-calculated using the post-collision velocities which are obtained by Eqs. (7) and (8).

To study the dependence of the inter-particle collision on the particle size, eight kinds of particles at the Stokes number of 0.01, 0.1, 0.5, 1, 5, 8, 10 and 100 are traced. Furthermore, the particle cluster, whose size distribution is corresponding with Rosin–Rammler distribution function (Macías-García et al., 2004; Giuliano et al., 2007), is also chosen as tracers to demonstrate the collision among particles with different sizes. For each case, 462 particles are injected into the flow-field every six time intervals. Initially, the particles are distributed uniformly in the nozzle and the velocity equal to the velocity of the local fluid.

3. Numerical results and discussions

3.1. Spatial distribution of the inter-particle collisions

Fig. 4 shows the spatial distribution of the inter-particle collisions at the Stokes number of 0.01, 0.1, 1, 10 and 100 in the flow field at the non-dimensional time $t = 42$, as well as the distributions of particles. In the figure, the red points represent the particles and the little green spheres represent the positions of inter-particle collisions. To observe the vortex structures interacting with the dispersed phase, the corresponding three-dimensional lateral vorticity are also shown in Fig. 4a. By comparison, the effects on dispersion of the particles having different Stokes number by vortex structures can be observed in detail. A brief summary of the particle dispersion patterns is provided here to explain

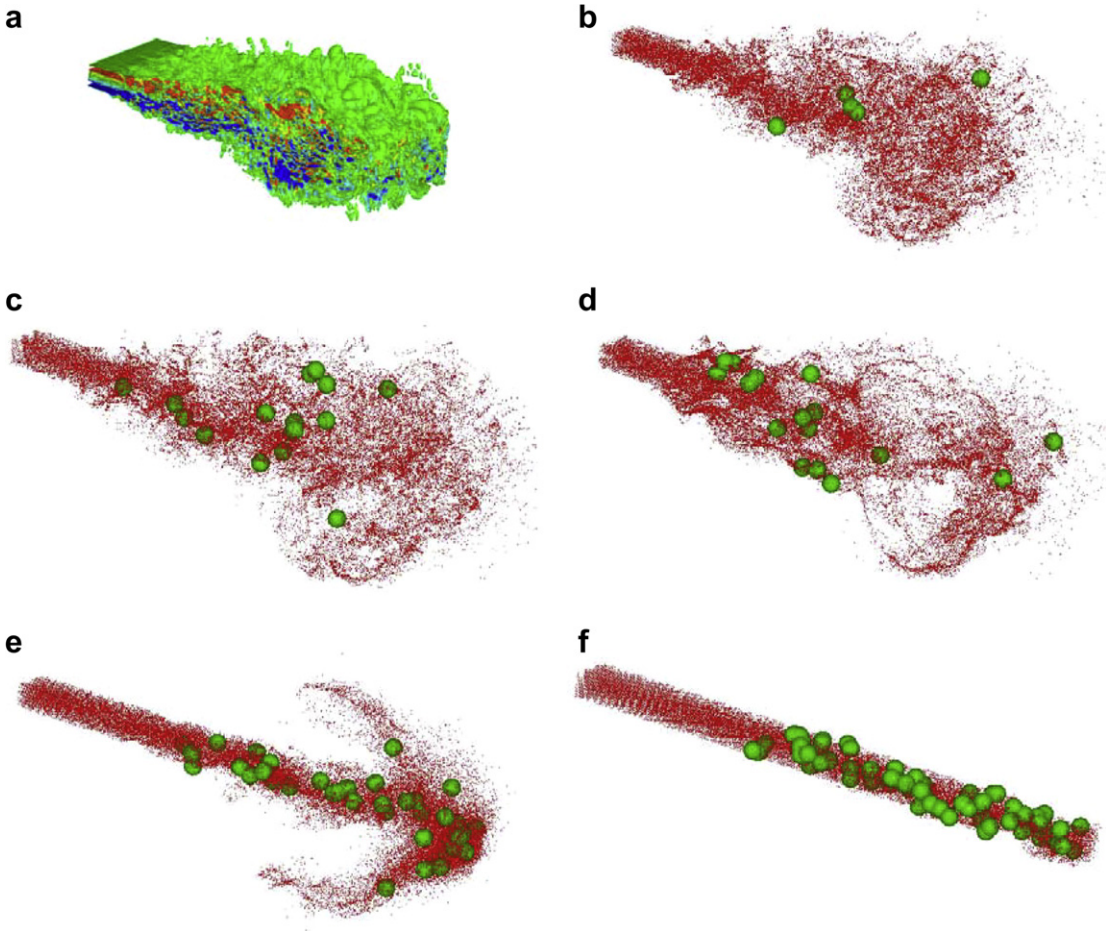

Fig. 4. Spatial distribution of inter-particle collision for particles at different Stokes numbers at the time $t = 42$. (a) Lateral vorticity, (b) $St = 0.01$, (c) $St = 0.1$, (d) $St = 1$, (e) $St = 10$, (f) $St = 100$.

the spatial distribution of the inter-particle collisions. However, the interested reader is referred to Luo et al. (2006) for additional details. At time $t = 42$, due to the coexistence of various vortex structures with different time scales and space scales in the flow field, the particle dispersion exhibits selective characteristic, i.e. the local particle concentration correlates well with the ratio of the aerodynamic response time of particles to the characteristic time of the local vortex structures. So, the particles having different Stokes number concentrate in different places (Chung and Troutt, 1988; Uchiyama and Naruseb, 2003). For particles having $St = 0.01$, because of the smaller aerodynamic response time scale, they can response quickly to fluid motion and are distributed uniformly in the flow field. Some particles can even disperse into the vortex core regions and form a similar uniform distribution to the vortex structures. This dispersion is consistent with the results of previous studies by Fan et al. (2004). Therefore, the phenomenon of inter-particle collisions for this kind of particles is not very obvious, as shown in Fig. 4b. The particles at the Stokes number of 0.1 can not disperse into the core regions any longer, most particles also distribute uniformly, but part of them concentrates in the inner boundaries of the large-scale structures. The inter-particle collisions are obvious in these regions, as shown in Fig. 4c. For $St = 1$, the particles concentrate largely in the outer boundaries of the large-scale vortex structures. In these regions where the local-focusing phenomenon happens, the inter-particle collisions can be found, as shown in Fig. 4d. Most particles at Stokes number of 10 move downstream through the vortex structures, and part of them disperses towards the upper and lower sides with some angle. So the inter-particle collisions not only happen in the center regions of the jet but also in both sides of the dispersion, as shown in Fig. 4e. When the Stokes number reaches 100, the particles are influenced less by the vortex structures and most particles directly move through the center regions of the jet towards down stream with nearly rectilinear paths. Consequently, the inter-particle collision positions are mainly in the center regions of the jet, as shown in Fig. 4f.

Fig. 5 shows the spatial distribution of collisions for particles at the Stokes number of 10 in the flow field at different times. Also, the corresponding three-dimensional lateral vorticities are shown to observe the vortex structures interacting with the dispersed phase. In the initial stage of the jet, due to the larger inertia, this kind of particles has not responded rapidly to the fluid motion and the lateral dispersion is small with local concentration regions. In these regions, the inter-particle collisions are prominent, as shown in Fig. 5a. The large-scale vortex structures are dominant at the non-dimensional time $t = 26$ and 34. The lateral dispersion of the particles can be observed in the down stream of the jet, some particles disperse towards the upper and lower sides with some angle. In this case, besides in the center regions of the jet, the local inter-particle collisions happen in both sides of dispersion, as shown in Fig. 5b and c. With the transition of the vortex structures from large-scale to small scale in the flow field, the particles move towards down stream at higher speed and form the considerable ellipse profile. However, the number of particles which disperse towards two sides is less and most particles move downstream through the vortex core regions. The reason is that the characteristic time scale of the particles is substantially larger than that of the vortex structures during the turbulence transition. Then, the particles are influenced less and less by vortex structures. As a result, the inter-particle collision positions are mainly in the center regions of the jet, as shown in Fig. 5d and e. These results suggest that the phenomenon of the inter-par-

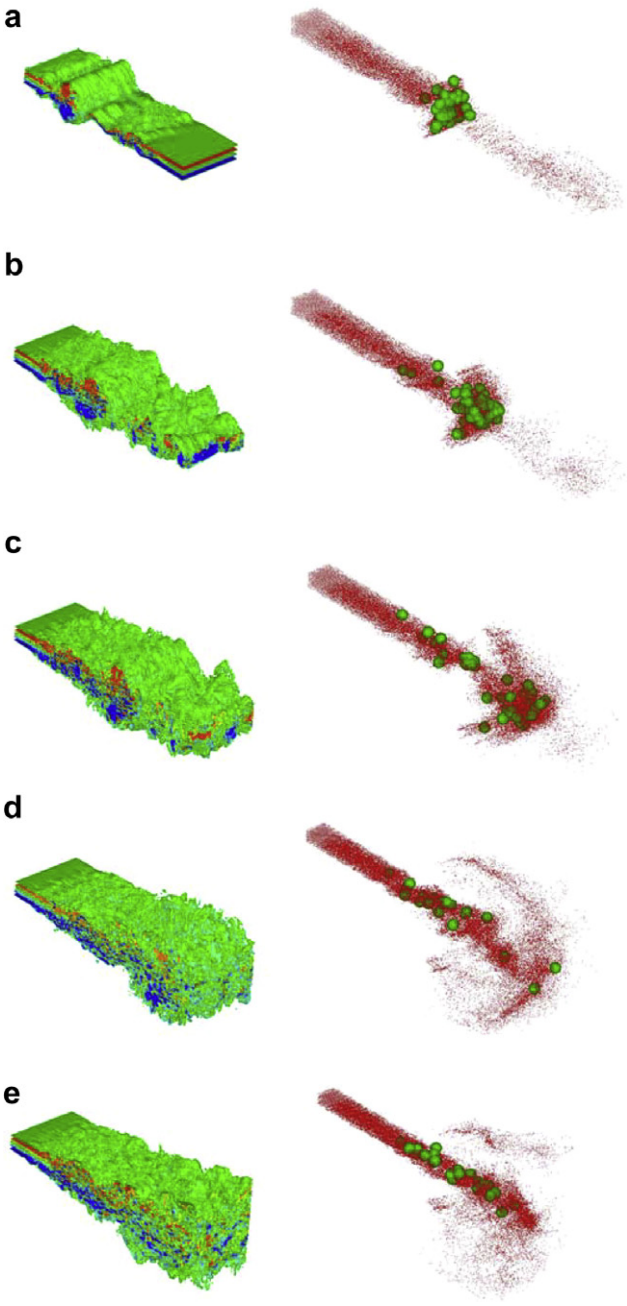

Fig. 5. Spatial distribution of vorticities and inter-particle collision for particles at the Stokes number of 10 at different times. (a) $t = 18$, (b) $t = 26$, (c) $t = 34$, (d) $t = 50$, and (e) $t = 74$.

ticle collision correlates well with the dispersion patterns of particles and the local particle concentration. Though the average concentration of the particles is lower in whole flow field, the inter-particle collisions are remarkable in the regions of local higher particle concentration.

3.2. Collision number

To further quantitatively investigate the effect on the inter-particle collision by the particle Stokes number, an important parameter, the average inter-particle collision number and its variation with the Stokes number is depicted in Fig. 6. Here the average inter-particle collision number is defined by $N_a = \frac{N}{\Delta t}$, where N is the total collision number during the time step Δt. It is clear that the average inter-particle collision number is not the simple linear relationship with the Stokes number. At $St = 0.1$, the average inter-particle collision number reaches a local peak value. After this, the average inter-particle collision number decreases and then turns to increase gradually with the increasing of the Stokes number. This complex behaviour is related to two foundational factors, both of which cause the intersection of particle trajectories and the occurrence of inter-particle collision: (i) particles tend to collect in regions of low vorticity leading to the changes of the local particle concentration and (ii) particle inertia affects the relative motion between neighboring particles thus altering their relative velocity. In this paper, the influence of both factors on the inter-particle collision is, respectively, termed the accumulation effect and the turbulent transport effect, followed Wang et al. (2000). Both of these effects will be presented.

As mentioned previously, the dispersion of particles having different Stokes number exhibits selective characteristic. In general, particles tend to assemble in the low-vorticity and high-strain regions (Chung and Troutt, 1988; Uchiyama and Naruseb, 2003; Fan et al., 2004; Luo et al., 2006). Particles with moderate Stokes number compared to the larger Stokes number are more susceptible to accumulation. Hence, they spend more time in the local regions of accumulation. For these particles, the inter-particle collision is mainly determined by the local accumulation effect and the relative motion between them is of second importance. Especially, the particles having $St = 0.1$ are more susceptible to accumulation due to the aerodynamics response time scale of them may be in the same order of the characteristic time scale of small-scale vortex structures and are driven predominantly by the small-scale vortex structures. The effect due to the local accumulation (i.e. the preferential concentration effect) reaches a maximum for the particles having $St = 0.1$ with the transition of vortex structures from large-scale to small scale, and thus, the local concentration of particles increases significantly with the development of jet and the inter-particle collisions are remarkable in these regions of local higher particle concentration. As a result, the average inter-particle collision number reaches a local peak value at $St = 0.1$. For $St = 1$, the aerodynamics response time scale of particles is close to the characteristic time scale of large-scale vortex structures. So the local concentration effect occurs only in the initial stage of the jet (a shorter time), when the large-scale vortex structures are in dominant. But with development of the flow field, the preferential concentration of the particles having $St = 1$ does not occur prominently and the concentration distribution of the particles also becomes uniform when large-scale structures change to small-scale. Consequently, the average inter-particle collision number in the whole stage of jet becomes small. However, the particles with larger Stokes numbers (e.g. $St > 5$) are influenced less and less by the fluid and unable to follow the fluid motion due to the larger inertia. They tend to collide more frequently because their inertia keeps them moving towards each other despite drag. In other words, the effect due to the local accumulation decreases for particles with larger Stokes numbers, and the turbulent transport effect starts to be the dominant factor contributing to the occurrence of inter-particle collision. Additionally, most of the particles having $St = 5$ or more directly move through the center regions of the jet towards down stream with small dispersion and thus the distance between particles decrease, which can easily cause the intersection of particle trajectories and thus causes the occurrence of inter-particle collision. Therefore, these particles collision number increases evidently.

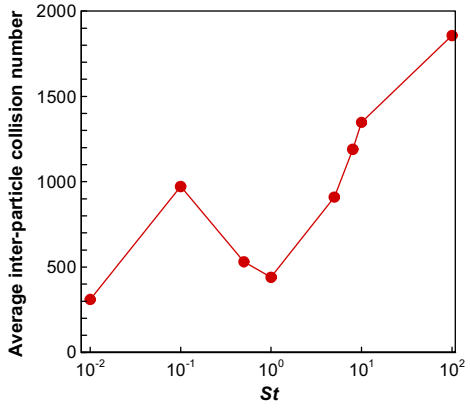

Fig. 6. Variation of the average inter-particle collision number with the Stokes number.

To investigate the evolution of the inter-particle collision with time, Fig. 7 shows the time history of the collision number and maximum particle number in the cell for typical particles at different Stokes numbers. The large-scale vortex structures are dominant in the early stage of the jet, the maximum particle number for each kind of particles in the cell increases linearly with t. So the inter-particle collision number also increases linearly with time during this period. After that, because the large particles for $St = 10$ and 100 are influenced less by the fluid, most particles move towards down stream with higher velocity. Along with this trend, the inter-particle collision number in the flow field also changes with the same patterns. But for the particles

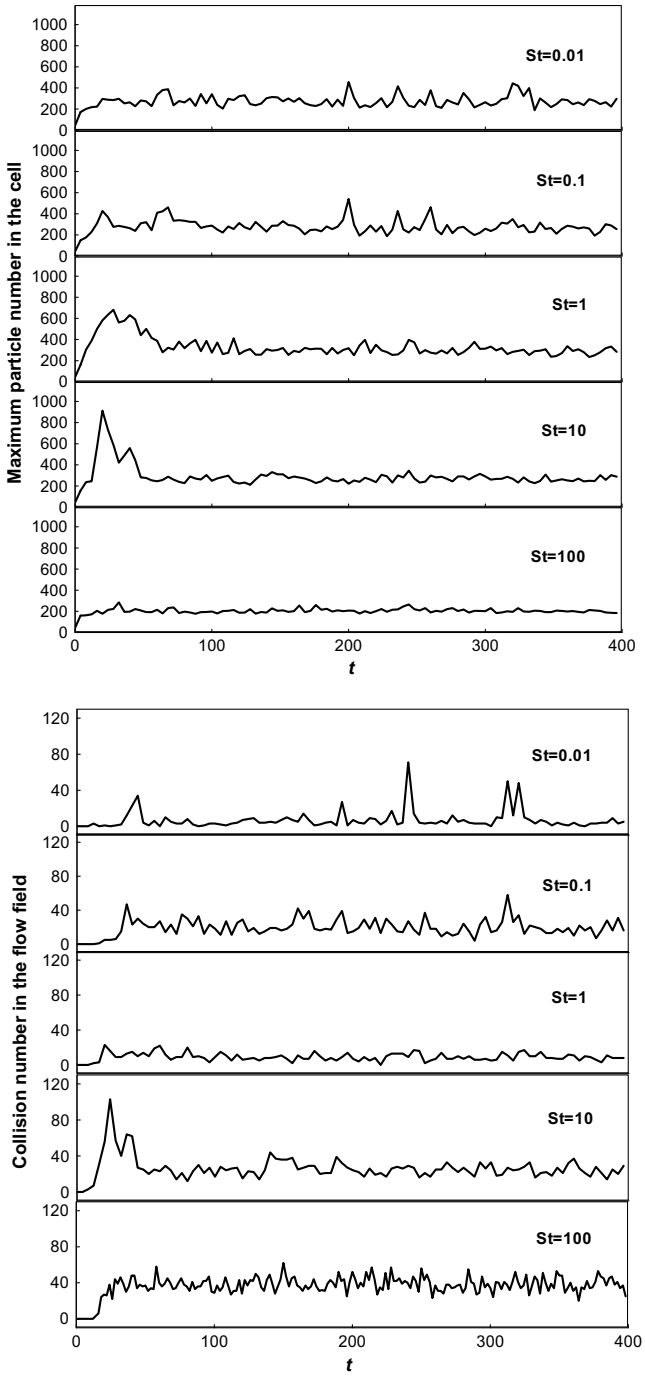

Fig. 7. Time history of the collision number and maximum particle number in the cell for particles at different Stokes numbers. (a) Maximum particle number in the cell; (b) collision number in the flow field.

with $St = 0.01$, 0.1 and 1, their dispersion are influenced greatly by the vortex structures. Due to the coexistence of various vortex structures with different time scales and space scales in the down stream of the jet, these particles adjust their dispersion patterns to exhibit selective dispersion characteristic. Then the preferential concentration effect occurs and the distribution of particles becomes non-uniform. Consequently, the maximum particle number in the cell for these particles is obviously fluctuant and reaches several evident peak values during the period of time $t = 200$–300, as shown in Fig. 7a. The collision number for these particles in the flow field also displays the corresponding variation. It is also found from Fig. 7 that though the concentration of particles with Stokes number of 100 in the cell is lower and fluctuant with little change, its collision number is higher. One explanation is the dispersion of large particles is lower and the relative motions of these particles become relatively significant due to the influence of large-scale energetic eddies, the turbulent transport effect is the dominant factor leading to the higher inter-particle collision number. This is in agreement with the conclusion showed in Fig. 6.

3.3. Effect of collision on particle dispersion

We regarded particles at Stokes number of 10 as representatives to quantitatively examine the effects of inter-particle collision. Cases with and without collision were calculated. The root mean square function of particle number per cell $N_{\mathrm{rms}}(t)$, the ratio of the particle number which is greater than 2 in single cell to the total particle number α are defined as

$$N_{\mathrm{rms}}(t) = \sqrt{\frac{\sum_{i=1}^{n_t} n_i(t)^2}{n_t}} \tag{12}$$

$$\alpha = \sum_{i=1}^{n(N)} N/N(t)(N > 2) \tag{13}$$

where n_t is the total number of computational cells in the statistical domain, $n_i(t)$ is the number of particles in the ith cell at the same time. N is the number of particles in certain cell, $n(N)$ is the number of cells with the particle number N, $N(t)$ is the total number of particles in the flow field at the time t. The function $N_{\mathrm{rms}}(t)$ can reflect the non-uniform of particle distribution in the flow field; the value of α can also reflect concentration distribution characteristics of particles.

To facilitate a comparison in later section, the developments of the root mean square function of particle number per cell and α with time for particles at the Stokes number of 10 are presented in Figs. 10 and 11 (in Section 3.4), respectively. The inter-particle collisions affect the profiles, i.e. the calculated results with inter-particle collisions are smaller than those without collisions. This indicates the distribution of particles in the flow field and in the cell becomes more uniform due to inter-particle collision. Especially in the initial stage of the jet, the concentration distribution of particles is the most non-uniform, and the inter-particle collision occurs very frequently due to the influence of the local accumulation and the turbulent transport effects. Consequently, the effect of the collisions on the statistic results is more obvious in the period of time $t = 20$–50, as shown in Fig. 10. The reason is that inter-particle collision causes the changes of the position and instantaneous velocity of particles and leads to more uniform particle distribution in the flow field.

3.4. Inter-particle collision with different Stokes numbers

In the above investigation, the inter-particle collision with the same Stokes number in each case was shown. In this section, the inter-particle collision is studied for the particle cluster with different Stokes numbers, that is, each of the particle may be a different size. Particle-size distribution is given by applying the most common Rosin–Rammler distribution function, which is expressed as

$$F(d) = 1 - \exp\left[-\left(\frac{d}{d_{50}}\right)^{m}\right] \tag{14}$$

where $F(d)$ is the distribution function, d is the particle size, d_{50} is the particle size corresponding with $F(d_{50}) = 0.5$, namely the medial particle size, and m is a measure of the spread of particle sizes. Here d_{50} and m are the adjustable parameters for different characteristics of the distribution. In this section, the particles with the size distribution demonstrated in Fig. 8 as weight percent amount in each size are traced. Here $d_{50} = 36.7$ μm, corresponding to the particles at the Stokes number of 10.

Fig. 9 shows the comparison of collision number for the particles with the Rosin–Rammler distribution ($d_{50} = 36.7$ μm) and the particles at the Stokes number of 10. It can be seen that both the variations of the collision number with time are basically the same, but the average collision number of the particles with the Rosin–Rammler distribution is significantly larger than that of the particles at the Stokes number of 10. This is because the particles with different sizes have different velocities, which easily cause the intersection of particle trajectories and make the particles to collide frequently.

The effects of inter-particle collision on particle distribution for these particles with different sizes are also investigated. Figs. 10 and 11 show the development of the root mean square function of particle number per cell and α with time separately. The inter-particle collision affects these profiles and the calculated results considering inter-particle collision are remarkably smaller than those without at the same time. This indicates that inter-particle collision makes the distribution of particles in the flow field become more uniform. These results are in good agreement with those corresponding to the particles having $St = 10$. Furthermore, the effects of inter-particle collision on the statistic results in the case of particles with different Stokes numbers becomes more significant compared with the effects of that in the case of particles at the Stokes number of 10. It is mainly associated with the more frequent inter-particle collision when a particle size distribution is applied. Because the velocities and trajectories of particles

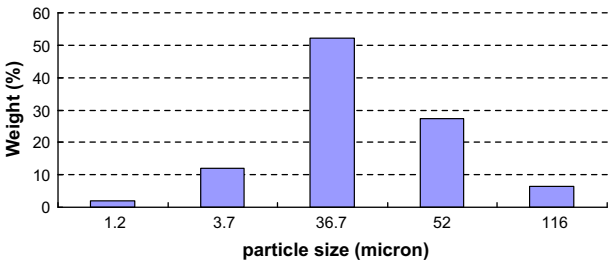

Fig. 8. Particle size distribution according to the Rosin–Rammler distribution function.

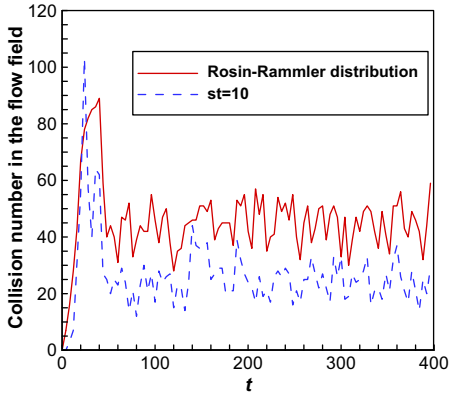

Fig. 9. Comparison of collision number for the particles according to the Rosin–Rammler distribution ($d_{50} = 36.7$ μm) and the particles at Stokes number of 10.

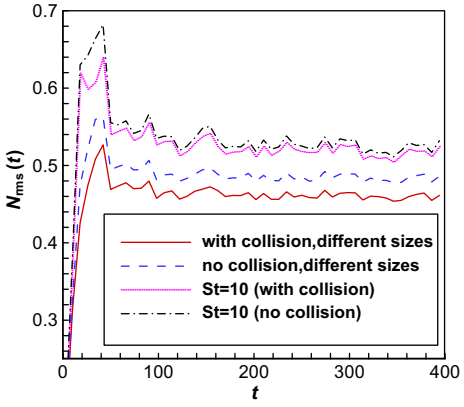

Fig. 10. Development of the root mean square function of particle number per cell for particles.

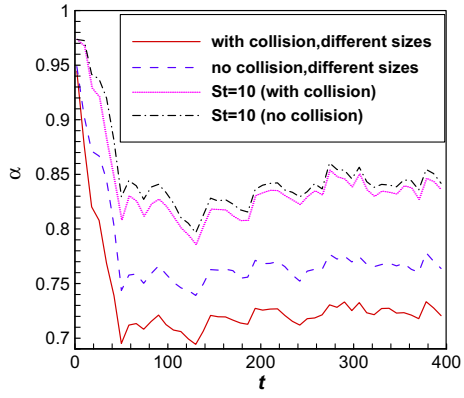

Fig. 11. Development of α for particles.

are various when there is a size distribution, small particles are more likely to collide with big particles than particles having the same size. As a result, the inter-particle collision is easier to happen for these particles having the different sizes.

Moreover, in order to quantitatively examine the effects of inter-particle collision on dispersion characteristics of particles along the lateral and the spanwise directions when there is a size distribution, the lateral dispersion function and the spanwise dispersion function are defined as

$$D_y(t) = \sqrt{\sum_{i=1}^{N(t)} (y_i(t) - y_{i0})^2 / N(t)} \tag{15}$$

$$D_z(t) = \sqrt{\sum_{i=1}^{N(t)} (z_i(t) - z_{i0})^2 / N(t)} \tag{16}$$

where $N(t)$ is the total number of particles in the flow field at the time t. $y_i(t)$ and $z_i(t)$ are, respectively, the lateral and spanwise displacements of the ith particle. and z_{i0} are the initial displacements of the ith particle when it is injected into the jet. The lateral dispersion function $D_y(t)$ and the spanwise dispersion function $D_z(t)$ denote the dispersion level of particles along the lateral and spanwise direction deviated from the center of jet, respectively.

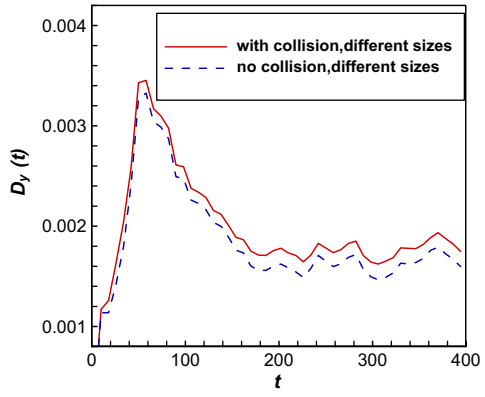

Fig. 12. Time history of the lateral dispersion function for the particles with different Stokes numbers.

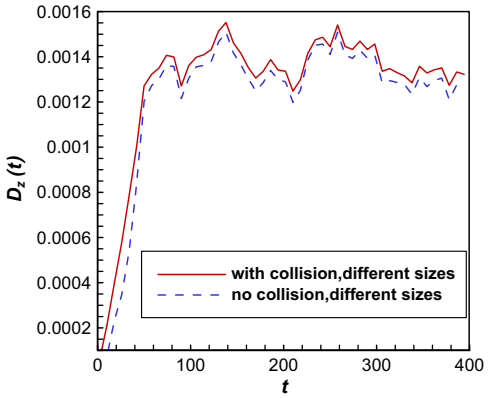

Fig. 13. Time history of the spanwise dispersion function for the particles with different Stokes numbers.

Figs. 12 and 13 show the time history of the lateral and spanwise dispersion function for particles having the different sizes. The values of the lateral and spanwise dispersion functions with inter-particle collision are both greater than those without. This demonstrates the lateral and the spanwise dispersion of the particles increase due to the effect of inter-particle collision in general. This agrees with the conclusions mentioned above that inter-particle collision makes the distribution of particles become more uniform in the flow field.

4. Conclusions

In summary, a detailed study of the inter-particle collision and its effects on the particle dispersion in a three-dimensional spatially evolving plane jet was presented based on direct numerical simulation and the deterministic hard-sphere model. The spatial distribution of instantaneous inter-particle collision for particles at the different Stokes numbers and the development of inter-particle collision number with the Stokes number and time were visualized. It is found that the occurrence of the inter-particle collision correlates well with the local particle concentration, though the average concentration of the particles is lower in the whole flow field. The relation between the average inter-particle collision number and the Stokes number is not the simple linear, but has a local maximum. First, the average inter-particle collision number increases to a local peak value, then turn to decline, and finally increases again gradually with the increasing of Stokes number. For particles at the same Stokes number, the variation of the collision number with time in the flow field is basically accordant with that of the maximum particle number in the cell with time.

Due to the effect of inter-particle collision, the particle distribution is more uniform and the lateral and the spanwise dispersion of the particles also are enhanced. For the particles according to the Rosin–Rammler distribution (the medial particle size is set $d_{50} = 36.7$ μm, corresponding to the particles at the Stokes number of 10), their collision number is significantly larger than that of the particles at the Stokes number of 10, and their effects on the statistical results are also more significant. According to the above conclusions, the inter-particle collision cannot be neglected even in the dilute turbulent jet.

Acknowledgement

The present work is supported by the National Nature Science Foundation of China (Grant Nos. 50506027 and 50736006). We are grateful to that.

References

Abrahamson, J., 1975. Collision rates of small particles in a vigorously turbulent fluid. Chem. Eng. Sci. 30, 1371–1379.

Bird, G.A., 1976. Molecular Gas Dynamics. Clarendon.

Chorin, A.J., 1968. Numerical solution of the Navier–Stokes equations. Math. Comput. 22, 745–762.

Chung, M.K., Troutt, T.R., 1988. Simulation of particle dispersion in an axisymmetric jet. J. Fluid Mech. 186, 199–222.

Clift, R., Grace, J.R., Weber, M.E., 1978. Bubbles, Drops, and Particles. Academic Press, New York.

Crowe, C.T., Gore, R.A., Troutt, T.R., 1985. Particle dispersion by coherent structures in free shear flows. Particul. Sci. Technol. 3, 149–158.

Crowe, C.T., Chung, T.N., Troutt, T.R., 1988. Particle mixing in free shear flows. Prog. Energy Combust. Sci. 14, 171–194.

Eaton, J.K., Fessler, J.R., 1994. Preferential concentration of particles by turbulence. Int. J. Multiphase Flows 20, 169–209.

Fan, J.R., Luo, K., Ha, M.Y., Cen, K.F., 2004. Direct numerical simulation of a near-field particle-laden plane turbulent jet. Phys. Rev. E 70, 026303.

Giuliano, V., Pagnanelli, F., Bornoroni, L., Toro, L., Abbruzzese, C., 2007. Toxic elements at a disused mine district particle size distribution and total concentration in stream sediments and mine tailings. J. Hazard. Mater. 148, 409–418.

Hardalupas, Y., Taylor, A.M.P.K., Whitelow, J.H., 1989. Velocity and particle-flux characteristics of turbulent particle laden jets. Proc. R. Soc. Lond. A 426, 31–78.

Klein, M., Sadiki, A., Janicka, J., 2003a. A digital filter based generation of inflow data for spatially developing direct numerical or large eddy simulations. J. Comput. Phys. 186, 652–665.

Klein, M., Sadiki, A., Janicka, J., 2003b. Investigation of the influence of the Reynolds number on a plane jet using direct numerical simulation. Int. J. Heat Fluid Flow 24, 785–794.

Longmire, E.K., 1994. Active open-loop control of particle dispersion of round jets. AIAA J. 32, 555–563.

Longmire, E.K., Eaton, J.K., 1992. Structure of a particle-laden round jet. J. Fluid Mech. 236, 217–257.

Lun, C.K.K., Liu, H.S., 1997. Numerical simulation of dilute turbulent gas–solid flows in horizontal channels. Int. J. Multiphase Flows 23, 575–605.

Luo, K., Klein, M., Fan, J.R., Cen, K.F., 2006. Effects on particle dispersion by turbulent transition in a jet. Phys. Lett. A 357, 345–350.

Macías-García, A., Cuerda-Correa, E.M., Díaz-Díez, M.A., 2004. Application of the Rosin–Rammler and Gates–Gaudin–Schuhmann models to the particle size distribution analysis of agglomerated cork. Mater. Charact. 52, 159–164.

Melville, W.K., Bray, K.N.C., 1979. A model of the two-phase turbulent jet. Int. J. Heat Mass Transfer 22, 647–656.

Oesterlé, B., Petitjean, A., 1993. Simulation of particle-to-particle interactions in gas–solid flows. Int. J. Multiphase Flows 19, 199–211.

Saffman, P.G., Turner, J.S., 1956. On the collision of drops in turbulent clouds. J. Fluid Mech. 1, 16–30.

Sakiz, M., Simonin, O., 2001. Continuum modelling and Lagrangian simulation of massive frictional colliding particles in a vertical gas–solid channel flow. In: Michaelides, E. (Ed.), Proceedings of the Fourth International Conference on Multiphase Flow. New Orleans, USA (CD-ROM Proc. ICMF_2001, Paper 186).

Sommerfeld, M., 1995. The importance of inter-particle collisions in horizontal gas–solid channel flows. In: Stock, D.E. et al. (Eds.), Gas–Particle Flows. ASME Fluids Engineering Conference, Hiltons Head, USA, FED-Vol. 228, ASME, pp. 335–345.

Sommerfeld, M., 2001. Validation of a stochastic Lagrangian modelling approach for inter-particle collisions in homogeneous isotropic turbulence. Int. J. Multiphase Flows 27, 1829–1858.

Sommerfeld, M., 2003. Analysis of collisions effects for turbulent gas-particle flow in a horizontal channel: Part I. Particle transport. Int. J. Multiphase Flows 29, 675–699.

Sommerfeld, M., Zivkovic, G., 1992. Recent advances in the numerical simulation of pneumatic conveying through pipe systems. In: Hirsch, Ch., Periaux, J., Onate, E. (Eds.), Computational Methods in Applied Science. Invited Lectures and Special Technological Sessions of the First European Computational Fluid Dynamics Conference and the First European Conference on Numerical Methods in Engineering, Brussels, pp. 201–212.

Stock, D.E., 1996. Particle dispersion in flowing gases-1994 Freeman scholar lecture. Trans. ASME 118, 4–17.

Sundaram, S., Collins, L.R., 1996. Numerical considerations in simulating a turbulent suspension of finite-volume particles. J. Comput. Phys. 124, 337–350.

Sundaram, S., Collins, L.R., 1997. Collision statistics in an isotropic particle-laden turbulent suspension I. Direct numerical simulations. J. Fluid Mech. 335, 75–109.

Tanaka, T., Tsuji, Y., 1991. Numerical simulation of gas–solid two-phase flow in a vertical pipe: on the effect of inter-particle collision. ASME/FED Gas–Solid Flows 121, 123–128.

Uchiyama, T., Naruseb, M., 2003. Vortex simulation of slit nozzle gas-particle two-phase jet. Powder Technol. 131, 156–165.

Vojir, D.J., Michaelides, E.E., 1994. Effect of the history term on the motion of rigid spheres in a viscous fluid. Int. J. Multiphase Flows 20, 547–556.

Wang, L.P., Wexler, A.S., Zhou, Y., 1998a. On the collision rate of small particles in isotropic turbulence I. Zero-inertia case. Phys. Fluid 10, 266–276.

Wang, L.P., Wexler, A.S., Zhou, Y., 1998b. On the collision rate of small particles in isotropic turbulence II. Finite inertia case. Phys. Fluid 10, 1206–1216.

Wang, L.P., Wexler, A.S., Zhou, Y., 2000. Statistical mechanical description and modeling of turbulent collision of inertial particles. J. Fluid Mech. 415, 117–153.

Wicker, R.B., Eaton, J.K., 2001. Structure of a swirling, recirculating coaxial free jet and its effect on particle motion. Int. J. Multiphase Flows 27, 949–970.

Yamamoto, Y., Potthoff, M., Tanaka, T., Kajishima, T., Tsuji, Y., 2001. Large-eddy simulation of turbulent gas-particle flow in a vertical channel: effect of considering inter-particle collisions. J. Fluid Mech. 442, 303–334.

Yonemura, S., Tanaka, T., Tsuji, Y., 1993. Cluster formation in gas–solid flow predicted by the DSMC method. In: Gas–Solid Flows, FED-Vol. 166, pp. 303–309.

Yuu, S., Ikeda, K., Umekage, T., 1996. Flow-field prediction and experimental verification of low Reynolds number gas-particle turbulent jets. Colloid Surf. A: Physicochem. Eng. Aspects 109, 13–27.